

# Near-infrared spectra of Seyfert galaxies and line production mechanisms

N. Jackson and R. J. Beswick

*The University of Manchester, Jodrell Bank Observatory, Macclesfield, Cheshire, SK11 9DL U.K.*

12 September 2018

## ABSTRACT

New observations are reported of  $J$ -band spectra ( $1.04\ \mu\text{m} - 1.4\ \mu\text{m}$ ) of three Seyfert 2 galaxies, Mkn 34, Mkn 78 and NGC 5929. In each case the spectral range includes the near-infrared lines of [FeII], [Pii], HeI and Pa $\beta$ . Each Seyfert galaxy has a known radio jet, and we investigate the infrared line ratios of the nuclear and extended regions of each galaxy compared to the radio structure. In Mkn 34 there is a clear indication of an extranuclear region, probably coincident with a shock induced by the radio jet, in which [FeII] is considerably enhanced, although the nuclear emission is almost certainly the result of photoionization by the continuum of the active nucleus. Similar effects in extranuclear regions are seen in the other objects, in the case of Mkn 78 confirming recent studies by Ramos Almeida et al. A possible detection of extranuclear [Pii] emission suggests, if real, that photoionization by the active nucleus is the dominant line excitation mechanism over the whole source, including the regions coincident with the radio jet.

**Key words:** galaxies:active – galaxies:individual:Mkn34 – galaxies:individual:Mkn78 – galaxies:individual:NGC5929 – line formation – infrared:galaxies

## 1 INTRODUCTION

Optical and near-infrared studies of nearby active galaxies can give us a lot of information about the physical processes taking place in these objects. Seyfert galaxies, as relatively nearby low-luminosity active galaxies, can be studied in particular detail. These objects contain emission lines within their spectrum, including in general broad lines produced within the inner parsec, close to the central black hole and accretion disk, and narrow lines whose region of production may extend over a kiloparsec. In addition, many Seyfert galaxies have weak radio emission, often in a linear structure corresponding to an outflow from the central active nucleus.

The physics of emission lines is of particular interest. These are thought mostly to arise through photoionization, and many studies have been done which use sophisticated photoionization models to reproduce emission lines in great detail. However, additional physics may be needed to reproduce some lines. In particular, the near-infrared [FeII] line at  $1.257\ \mu\text{m}$  has been suggested as a diagnostic of shock excitation, which may arise as dust grains are dissociated in fast shocks (e.g. Forbes & Ward 1993). The idea that shocks may have general applicability to AGN spectra was argued by Sutherland et al. (2003) and Dopita & Sutherland (1995) who succeeded in reproducing many characteristic photoionized spectra using shock models. This arises because shocks

generate UV and X-ray photons which can then ionize the gas – indeed, the difference between the observed properties of such “autoionizing” shocks and regions photoionized by a central active nucleus can be quite subtle and depend on the details of the spectra of the incident photons.

More recently, Simpson et al. (1996) showed that the observed [FeII] line is also consistent with predominantly being produced by photoionization, and Mouri, Kawara & Taniguchi (2000) conducted more sophisticated calculations suggesting that electron collisions in a partially-ionized zone associated with a shock may be the production mechanism rather than grain dissociation. Based on such studies, Alonso-Herrero et al. (1997) propose the use of the ratio of infrared [FeII] lines to the hydrogen recombination lines to separate active galaxies from starbursts. Oliva et al. (2001) studied the problem of shock ionization versus photoionization. They suggested that the [Pii] line is potentially useful in disentangling this problem, because similar physical conditions are needed to produce it to those which produce [FeII], but unlike iron, phosphorus is not produced in destruction of dust grains. A high Fe/P ratio is thus a prediction of models in which dust grains are dissociated by shocks. Oliva et al. find that pure photoionization better fits their spectrum of the very bright Seyfert galaxy NGC 1068. In fainter galaxies where [Pii] is not detected, even

lower limits on the Fe/P ratio may be useful in ruling out shock models if the spectra are sensitive enough.

Although Seyfert galaxies have been studied extensively in the optical, high signal-to-noise observations in the near-infrared are rarer. A compilation has recently been published by Riffel, Rodríguez-Ardila & Pastoriza (2006) including many of their own *JHK* spectra (Rodríguez-Ardila, Riffel & Pastoriza 2005). Many of these spectra suggest that the line ratio of active galaxies have a  $[\text{FeI}]/\text{H}\beta$  ratio suggestive of X-ray heating or regions of star formation. Recently, Ramos Almeida et al. (2006) have published infrared spectra of one of the objects discussed here, Mkn 78, and deduce from observations and simulations that the predominant line-excitation mechanism in the nuclear region is photoionization by the hard UV continuum from the active nucleus, although radio-induced shocks may contribute within one of the radio lobes.

In this work we choose objects in which linear radio structure is clearly seen in order to investigate the emission-line structure along the jet axis and look for evidence for shock excitation. If shocks are indeed an important part of the physics, the area where the radio jet is depositing energy into the interstellar medium is an obvious place to look. The spectra presented here are from deep exposures (1–2 hours with an 8-m class telescope) and therefore allow us to investigate both nuclear and off-nuclear emission.

## 2 OBSERVATIONS AND ANALYSIS

### 2.1 Infrared and optical data

All infrared observations were conducted using the 8-m Gemini-North Telescope, Mauna Kea, on the nights of 2005 February 17, February 18 and May 22 using the NIRI imaging spectrograph in f/6 spectroscopy mode. The J grism was used with a J-band order-sorting filter, giving a wavelength range of approximately  $1.05\mu\text{m} - 1.42\mu\text{m}$ , together with a 4-pixel slit which corresponds to  $0''.46$  on the sky and a resolving power of about 600 (Hodapp et al. 2003). Mkn 78 was observed for 2 hours on 2005 February 17, Mkn 34 for 2 hours on 2005 February 18 and NGC 5929 for 70 minutes on 2005 May 22. Each observation was divided into  $3 \times 30$  second exposures, and each successive exposure was chopped up and down the slit to make sky subtraction easier and minimize effects of bad pixels. Lamp flatfield exposures and argon arc exposures were also obtained for Mkn 34 and Mkn 78. In the case of NGC 5929, no argon lamp spectrum is available and in this case the atmospheric OH lines have been used for wavelength calibration.

Data reduction was performed using the Starlink FIGARO package and began with combination of the flatfields and division of the data frames by a flatfield normalised in the spectral direction. A second-order polynomial fit to at least six arc lines was obtained which gave a maximum error of 0.1 nm across the wavelength range. The spectra were corrected for S-distortion using three spectra of the Hipparcos stars taken at different positions on the chip. The sky was then subtracted using the Figaro task POLYSKY and the spectra extracted using the optimal extraction algorithm of Horne (1986) using the Figaro task OPTEXTRACT.

Relative flux calibration was performed assuming a

blackbody spectrum of 7200K for the Hipparcos F0V star HIP36366 (Perryman 1997) and temperatures of 7200K and 7000K for the stars HIP56601 and HIP75411 respectively. The  $\text{Pa}5 \rightarrow 3$ ,  $6 \rightarrow 3$  and higher order absorption bands were interactively edited out of the stellar spectrum before this process in order to avoid them appearing as emission lines in the divided spectrum.

For deriving velocity profiles, successive rows of the sky-subtracted image have been extracted, continuum-subtracted using line-free regions immediately around each line, and fitted with Gaussian profiles. Profile fitting has been done by software written by us, using the Levenberg-Marquardt algorithm as implemented by Press et al. (1992).

In addition to the infra-red data, some data from the Isaac Newton Group (ING) archive was extracted for the Seyfert galaxy Markarian 34. These data were taken using the William Herschel 4.2-m telescope on La Palma on 1998 December 17 using the ISIS two-arm spectrograph. On the red arm of this spectrograph the TEK-2 chip was used together with an R600R grating, using a  $1''.23$  slit and a resulting spectral resolution of just over 0.2nm. The data were co-added and fluxes of  $[\text{OI}]$  and  $\text{H}\alpha$  derived assuming a flat spectral response over this wavelength range, because both the TEK-2 chip and the R600R grating have a flat spectral response over this range to within a few percent.

### 2.2 Radio data

Complementary, mainly previously-published (Falcke, Wilson & Simpson 1998; Whittle & Wilson 2004) public domain radio data for each of these three sources were obtained and re-mapped for comparison purposes from the NRAO's Very Large Array (VLA) archive. In each case these data were observed at a wavelength 3.6 cm and in the VLA's highest resolution configuration, providing an angular resolution of  $\sim 0.2\text{--}0.3$  arcsec which is directly comparable to the spectroscopic observations presented. A brief summary of the observing parameters is given in Table 1. Each data-set was calibrated using standard data reduction techniques within NRAO's AIPS package where these data were edited before phase solutions from a nearby reference source were applied. In each case the flux density scale was calibrated with respect to 3C 286 using the Baars *et al.* (1977) scale.

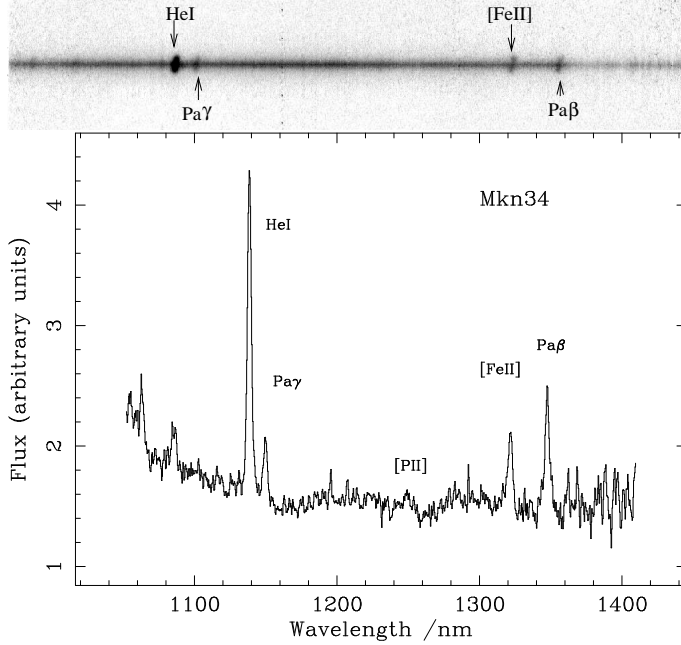
## 3 RESULTS AND LINE DIAGNOSTICS

### 3.1 Mkn 34 ( $z=0.0505$ )

Markarian 34 is a Seyfert 2 galaxy with a  $2''.4$  extended radio structure whose extended optical line emission has been studied in detail by Whittle et al. (1988) and Falcke, Wilson & Simpson (1998). Its off-nuclear line emission shows a velocity profile with relatively broad  $[\text{OIII}]$  emission extending slightly beyond the radio lobes. There is a distinct difference between the velocity of the line emission near to the nucleus and that beyond the radio lobes. The new infrared spectrum was taken with the slit at a position angle  $158^\circ$  East of North, coincident with the radio axis. Figure 1 shows the image of the spectrum along the slit, showing a clear rotation-type velocity profile in all securely detected lines ( $\text{HeI}$ ,  $[\text{FeI}]$ ,  $\text{Pa}\beta$  and  $\text{Pa}\gamma$ ).

**Table 1.** Summary of archival VLA observations.

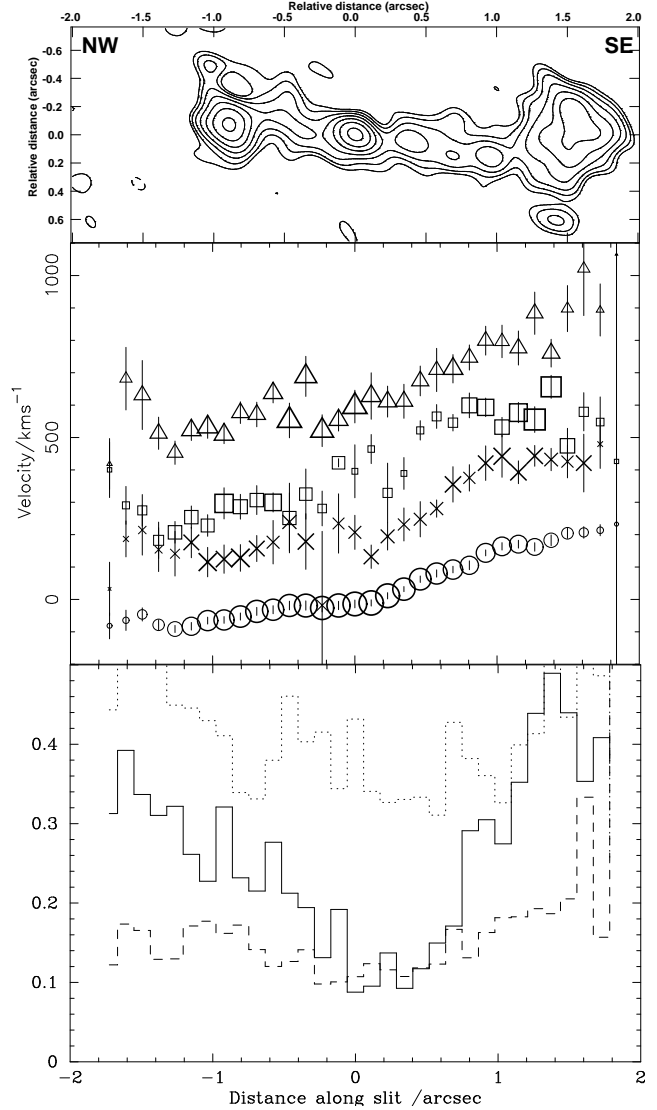
Source	Date	Phase ref.	Time on source	Original publication
Mkn 34	1996 Nov 4	1030+611	166 min	Falcke, Wilson & Simpson 1998
NGC 5929	2003 Jun 20	1506+426	8 min	
Mkn 78	1990 Apr 16	0716+714	340 min	Whittle & Wilson 2004


**Figure 1.** *J*-band spectrum of Mkn 34, showing the brightest emission lines.

[Pii] is detected at a marginal level in the nuclear spectrum. In the nuclear region, the ratio  $[\text{FeII}]\lambda 1.257/[\text{Pii}]$  is  $3.2 \pm 1.0$ , which is consistent with the range of values typical of nuclear photoionization (Oliva et al. 2001).

The radio map of Falcke et al. (1998) shows structure similar to that seen earlier by Ulvestad & Wilson (1984) at 6 and 20 cm, but with higher angular resolution and sensitivity shows the definition of the radio jet structure more clearly. In particular the jet is resolved into several discrete knots and a significant change in the projected position angle of the tip of the southeastern jet is seen.

The most striking feature of the spectrum is the different distribution between [FeII] and the other lines. Figure 2 illustrates the rotation curve and strength of the lines, and it is clear that [FeII] has a bright knot about  $1''.2$  to the SE. This is just behind the bright radio knot in the southeastern jet imaged here and by Whittle et al. (1988). Although the Paschen recombination lines are slightly enhanced in the off-nuclear regions compared to the nucleus, the ratio of [FeII]/Pa $\beta$  becomes a factor of 2–3 stronger away from the nucleus, suggesting that different ionization mechanisms may be operating here. The HeI line displays a different behaviour to the hydrogen recombination lines, showing a smooth decrease in each direction away from the nucleus with little sign of any increase in strength in the radio lobes.


**Figure 2.** Central panel: Velocity profile of Mkn 34. Four lines are shown, HeI (circles), Pa $\gamma$  (crosses), [FeII] (squares) and Pa $\beta$  (triangles). Line quantities have been measured by Gaussian fits to successive rows of the spectral image, and the amplitude within each sequence of line fits is proportional to the size of the symbol. Each successive line has been offset by  $200 \text{ km s}^{-1}$  for clarity. Note the clearly different pattern of the [FeII] emission from the other lines; it is highly concentrated in region of the SE radio knot. The radio map (top panel) from data presented by Falcke et al. (1998) is shown to the same scale, and rotated to the axis of the spectrograph slit. The bottom panel shows the line ratios compared to HeI of [FeII] (solid line), Pa $\gamma$  (dashed line) and Pa $\beta$  (dotted line).

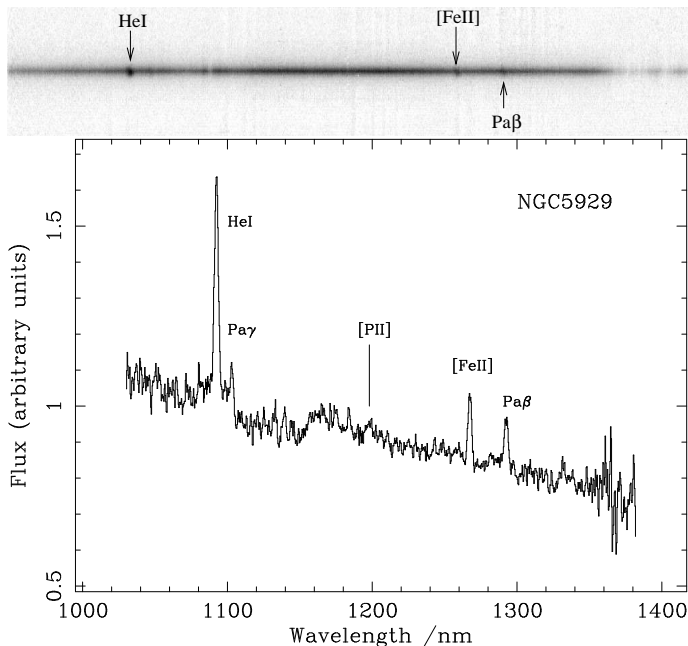


**Figure 3.** *J*-band spectrum of NGC 5929, showing the brightest emission lines.

### 3.2 NGC 5929 ( $z=0.00831$ )

NGC5929 is a Seyfert galaxy with a radio jet extending about  $0''.7$  in PA  $\sim 60^\circ$  either side of a compact nucleus (Su et al. 1996; Cole et al. 1998) and extended optical emission partly coincident with the western radio lobe (Bower et al. 1994), strongly suggesting an interaction. Nuclear infrared spectroscopy was performed by Simpson et al. (1996) who clearly detected the [FeII] line and found it to be marginally resolved. The current observations have a smaller pixel scale, and we clearly see the resolution in this object, using a slit at the position angle of the extended optical emission previously seen ( $65^\circ$ ). The nuclear spectrum is shown in Figure 3.

In the nuclear emission the [PII] line is detected at just over the  $3\sigma$  level; a previous spectrum reported by Rodríguez-Ardila, Riffel & Pastoriza (2005) and Riffel et al. (2006) did not detect this line. A Gaussian fit to the [FeII] and [PII] lines was carried out, constraining the [PII] line width to be equal to that of [FeII]. The [FeII]/[PII] ratio is  $4.3 \pm 1.1$  in the nuclear region, which again is typical of photoionized regions and considerably less than the value of  $\sim 20$  expected for shock ionization (Oliva et al. 2001). The [FeII]/Pa $\beta$  ratio is approximately 1, in agreement with the previous spectra.

Figure 4 shows the radio map; similar structure is seen to the earlier radio map of Su et al. (1996) and Cole et al. (1998) with a compact core and two lobe structures detected.

The most remarkable feature of the spectrum is the wholesale displacement of the line emission from the centre of the galaxy and of the velocity profile (Figure 5). This effect is extreme around the southwestern radio lobe, where the [FeII] line strength peaks. The HeI line peak is also offset, although by less than the [FeII]. Optical studies with the *Hubble Space Telescope* (Bower et al. 1994) have also revealed [OIII] emission which peaks around the southwest-

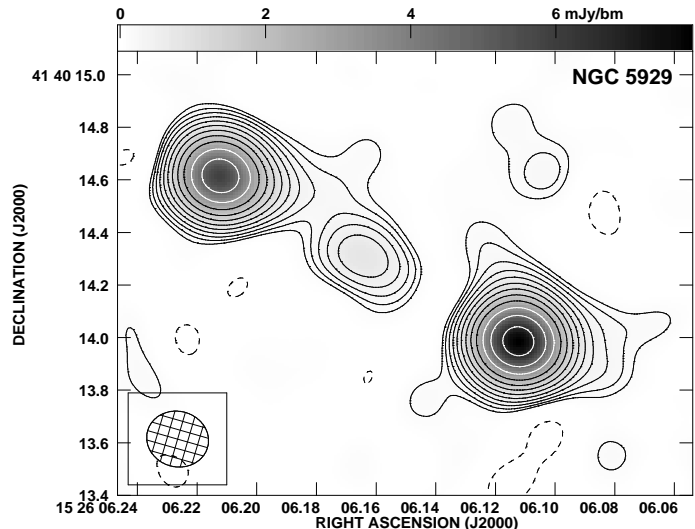


**Figure 4.** VLA 3.6cm image of NGC 5929, showing features similar to the map of Su et al. (1996). The map is contoured at multiples of  $\sqrt{2} \times 0.146 \text{ mJy bm}^{-1}$  ( $3\sigma$ ). The image has been convolved with Gaussian beam of  $0''.234 \times 0''.211$  with a of PA= $74^\circ$ .

ern radio lobe. Around the northeastern radio lobe, there is some evidence of disturbed kinematics in the [FeII] line.

### 3.3 Mkn 78 ( $z=0.03715$ )

Mkn 78 has recently been the subject of an extensive optical study with the Hubble Space Telescope by Whittle & Wilson (2004), Whittle et al. (2004) and Whittle et al. (2005) specifically directed at disentangling shock ionization and photoionization. This Seyfert galaxy has extended radio emission, in a linear structure about  $2''$  long in an E-W direction, and Whittle & Wilson (2004) have imaged a large and complex extended structure in [OIII] extending  $3''$  from the nucleus in each direction. In these observations the slit was aligned in PA  $90^\circ$  in the hope of detecting significant extended structure in the infrared emission lines. The nuclear spectrum of this object is shown in Figure 6, and the measurements of the extended emission and velocity profile are displayed in Figure 7.

In the optical observations of Whittle et al. (2005), very complex extended optical line emission was detected in all major recombination and forbidden lines. In these infrared observations, the structure is not well resolved either spatially or spectrally. However, the overall rotation curve is detected in extended emission in three major emission lines, HeI, [FeII] and Pa $\beta$ , covering about  $2''$  to the East of the nucleus. Relatively little line emission is seen to the West, which is also the direction of lower surface brightness in [OIII] from the maps of Whittle & Wilson (2004).

A recent detailed infrared study has been carried out with the LIRIS spectrograph on the William Herschel Telescope by Ramos Almeida et al. (2006). They find a nuclear ratio of [FeII]/Pa $\alpha$  which is consistent with photoionization from the active nucleus. Moreover, they detect [PII] in the nucleus at a strength that is a factor of 1.82 lower than the [FeII] $\lambda 1.644$  line. This ratio is also consistent with photoionization, being similar to the ratio found in NGC 1068 by Oliva et al. (2001), and is inconsistent with shock mod-

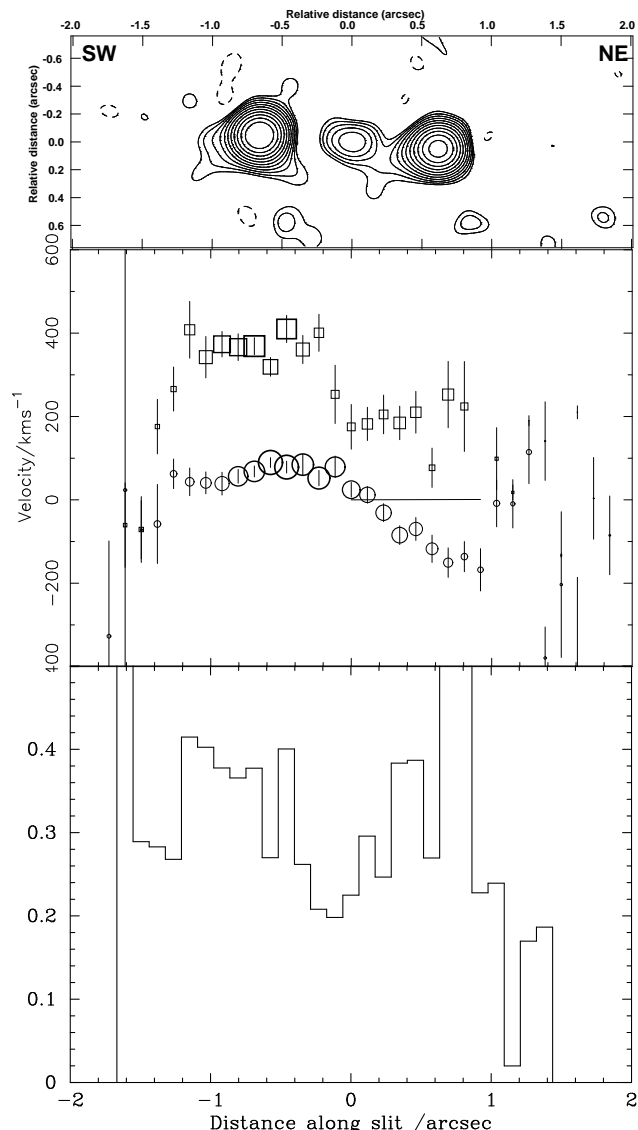


**Figure 5.** Central panel: Velocity profile of NGC 5929. Two lines are shown, HeI (circles) and [FeII] (squares). Line quantities have been measured by Gaussian fits to successive rows of the spectral image, and the amplitude within each sequence of line fits is proportional to the size of the symbol. Each successive line has been offset by  $200 \text{ km s}^{-1}$  for clarity. The radio map (top panel) is the same as Fig. 4, but is shown to the same scale, and rotated to the axis of the spectrograph slit. The bottom panel shows the variation of the line ratio [FeII]/HeI over the same scale.

els. However, in the extended emission associated with the western radio lobe, they find that the [FeII] line strength increases by a factor  $\sim 2$  relative to the hydrogen recombination lines, suggesting a contribution from interaction with the radio bow shock. We find a similar effect in our data, with an enhancement in [FeII] which peaks at  $\sim 0''.6$  from the nucleus. However, the association of increased [FeII] emission with the radio structure is *less* obvious in this object than in the other two in this study. In the western lobe the peak of the [FeII] does coincide with the W-knot of radio emission seen at higher resolution by Whittle et al. (2004) and shown in the superposed uniformly weighted image in the top panel of figure 7. The stronger, eastern radio jet is co-spatial with

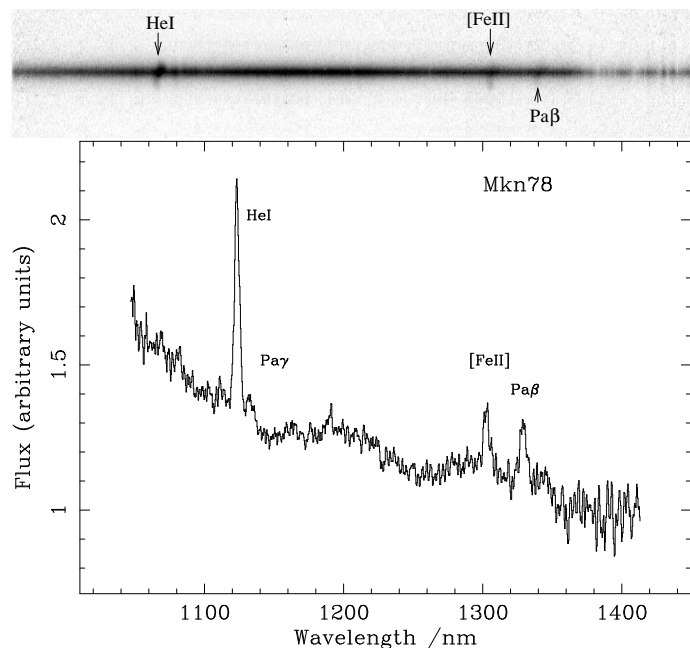


**Figure 6.** *J*-band spectrum of Mkn 78, showing the brightest emission lines.

a region in which the [FeII] (and Pa $\gamma$ ) emission becomes extremely faint and difficult to measure accurately. The HeI line displays different behaviour; as in Mkn 34, its strength decreases smoothly away from the nucleus. The Pa $\gamma$  line, although it can be followed for about  $2''$  either side of the nucleus, is not detected at high enough signal-to-noise to describe its structure in detail.

## 4 IONIZATION MECHANISMS AND DIAGNOSTICS

### 4.1 Nuclear emission: the [FeII]/[P1I] ratio

This paper adds to the total number of detections of [P1I] $\lambda 1.188\mu\text{m}$  in the literature. Since its original detection in NGC 1068 by Oliva et al. (2001) the line has been detected in the Seyfert 1 galaxy Akn 564 by Rodríguez-Ardila, Riffel & Pastoriza (2005), in Mkn 78 by Ramos Almeida et al. (2006), and in a total of 11 galaxies in the compilation of Riffel et al. (2006). Although very marginal, the detections of [P1I] in Mkn 34 and NGC 5929 suggest [FeII]/[P1I] ratios of 3–4, in agreement with ratios determined in other objects. Comparison with the models presented by Oliva et al. (2001) suggests that the dominant ionization mechanism is photoionization by the active nucleus rather than shock excitation; fast shocks would be expected to disrupt dust grains and produce line ratios a factor of 10 higher.

### 4.2 Extended emission

#### 4.2.1 Line diagnostic diagrams

There have been a number of investigations which have attempted to compare near-infrared line ratios with ionization codes. Many have used the CLOUDY code (Ferland et al. 1998) for a range of physical parameters, namely: density of

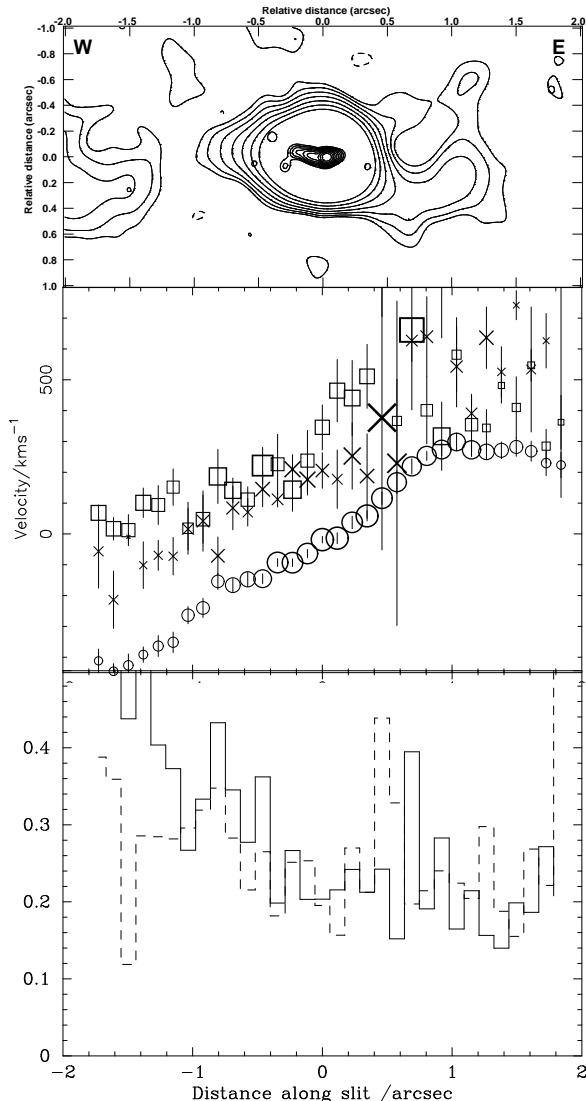


**Figure 7.** Velocity profile of Mkn 78. Three lines are shown, He I (circles), Pa $\beta$  (crosses), [Fe II] (squares). Line quantities have been measured by Gaussian fits to successive rows of the spectral image, and the amplitude within each sequence of line fits is proportional to the size of the symbol. Each successive line has been offset by 200 km s<sup>-1</sup> for clarity. The radio map (top panel) is made using the data of Whittle & Wilson (2004); it shows the central part of the radio emission, rotated to the axis of the spectrograph slit. Superposed on this radio map is a higher resolution (0''.075) uniformly weighted radio image of the core and inner jet. This inner image uses the same contouring scheme as the outer image with a lowest contour value contour of 0.1 mJy beam<sup>-1</sup>. The apparent high amplitude of the [Fe II] line at 0''.7 is the result of a noisy fit which is unlikely to be representative of the true flux; the same is true of the Pa $\beta$  line at 0''.45. The bottom panel shows the line ratios compared to He I of [Fe II] (solid line), and Pa $\beta$  (dashed line).

hydrogen, ionization parameter, ionizing power-law slope, metal abundance and presence or absence of dust grains (Simpson et al. 1996; Ramos Almeida et al. 2006). Others have used the MAPPINGS code or modifications to it (Sutherland et al. 1993; Mouri et al. 2000). Of particular interest is the ratio of [Fe II] to the other lines available in the near-

infrared spectrum, in particular the hydrogen recombination lines. Also interesting is the optical [O I] $\lambda$ 6300 line, as this has a similar ionization potential to [Fe II] and is produced in a partially-ionized zone with similar physical properties to the region producing [Fe II]. It can therefore serve as an alternative diagnostic of shock excitation to [P II]. Although much stronger than [P II], [O I] suffers from the disadvantage that the [O I]/[Fe II] ratio is subject to substantial reddening and is difficult to measure with the same instrument.

The effect of different physical parameters on the relative strengths of the [Fe II] and hydrogen recombination lines (in particular Pa $\beta$ ) can be summarized as follows (Simpson et al. 1996, Mouri et al. 2000; Ramos Almeida et al. 2006):

- Metal abundance changes the [Fe II]/Pa $\beta$  ratio by approximately the scaling of the abundance, for example by a factor of  $\sim 6$  from solar to Orion abundance.
- Neutral hydrogen density has relatively little effect, except at very high densities when the forbidden lines are in any case close to collisional de-excitation. For most values of ionization parameter, increasing densities decreases the relative strength of [Fe II] very slightly.
- Increasing ionization parameter causes a slow decrease in the [Fe II]/Pa $\beta$  ratio below  $U = 10^{-1.5}$ , and a rapid increase above this.
- The slope of the power-law has a drastic effect on the [Fe II]/Pa $\beta$  ratio; a steepening by 0.4 (from  $-1.0$  to  $-1.4$ ) typically halves the ratio, and the ratio becomes even smaller if a 40000-K blackbody model is adopted instead. This was considered in detail by Simpson et al. (1996), although Ramos Almeida et al. (2006) use an index of  $-2.0$  throughout their simulations.

In order to compare results with physical models and extract physical information from the line ratios, we have used the CLOUDY program (Ferland et al. 1998), version c06.02b. Models have been calculated for ionization parameters ranging from  $10^{-3.5}$  to  $10^{-1.5}$  in steps of  $10^{0.5}$  and electron densities between  $10^{3.5}$  and  $10^6$ , also in steps of  $10^{0.5}$ . For each combination of ionization parameter and density, two different metallicities ( $0.4Z_{\odot}$  and  $Z_{\odot}$ ) and two values of the spectral index of the power-law photoionizing continuum ( $-1$  and  $-2$ ) have been used. Grains were added to the simulation and were adjusted to be similar to Orion grains.

The diagnostic diagram of [Fe II] $\lambda$ 1.257/Pa $\beta$  vs. [O I]/H $\alpha$  is shown for Mkn 34 in Figure 8. This is the same diagram as presented in Figure 3 of Mouri et al. (2000). The trends in line ratio with ionization parameter, hydrogen density and slope of the ionizing continuum agree with previous determinations. In particular, an increase in ionization parameter causes decreases in both the [Fe II] $\lambda$ 1.257/Pa $\beta$  and the [O I]/H $\alpha$  ratio of about the same magnitude, provided that the slope of the ionizing continuum, is relatively steep ( $< -1.5$ ); in practice, relatively steep continua are needed to fit these data.

We have already noted that the ratio between [Fe II] $\lambda$ 1.257 and the hydrogen recombination lines increases in the objects studied as one moves from the nuclear regions to the areas associated with radio lobe emission. In principle, if the sole mechanism operating is ionization by hard-UV radiation from an active nucleus, this change in line ratio could be caused by a decrease in ionization parameter resulting from a geometrical dilution in the ionizing photon

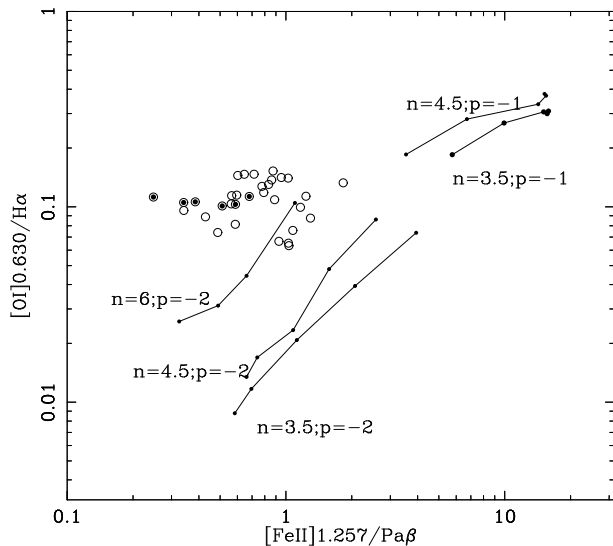


**Figure 8.** Diagnostic diagram of  $[\text{FeII}]\lambda 1.257/\text{Pa}\beta$  vs.  $[\text{OI}]/\text{H}\alpha$  compared to the observations of Mkn 34. Observational values (circles) within  $2''$  either side of the nucleus are shown, and pixels  $<0''.4$  from the nucleus are shown as solid blobs surrounded by a circle. Model tracks from the CLOUDY program are also shown, for various values of the ionizing continuum power-law slope ( $p$ ), hydrogen density ( $n$ , in  $\log_{10}\text{cm}^{-3}$ ). All tracks are calculated for  $Z = 0.4Z_{\odot}$ . Within each track, the ionization parameter  $U$  varies from  $-1.5$  to  $-3.5$ , with the higher values of  $[\text{FeII}]\lambda 1.257/\text{Pa}\beta$  occurring at lower  $U$ .

flux or an increase in the electron density associated with compression by the radio jet. This is indeed the conclusion of Falcke et al. (1998) who study the variation of the  $[\text{OIII}]/\text{H}\alpha$  ratio and find that it decreases away from the nucleus. In this case, however, one would also expect the  $[\text{OI}]/\text{H}\alpha$  ratio to increase, and this does not seem to be the case (Figure 8). In fact, this ratio is actually smaller in the southeastern lobe of Mkn 34, where the strongest interaction may be taking place, than in the nucleus of Mkn 34. Since the  $[\text{OI}]$  and  $[\text{FeII}]$  lines are produced in the same type of partially ionized zone and in similar physical conditions, the lack of correlation between their ratios to hydrogen recombination lines is puzzling.

The same, however, does not appear to be the case in Mkn 78. Whittle et al. (2005)’s extensive study of the extended optical emission lines in this object suggest that all lines, including  $[\text{OI}]$ , follow standard tracks from photoionization diagnostics, with a variation of about a factor of 10 in  $U$ ; this is sufficient to produce a difference of about a factor of 2 in  $[\text{FeII}]\lambda 1.257/\text{Pa}\beta$ .

Images of some optical emission lines in the extended regions of NGC 5929 are presented by Bower et al. (1994) and discussed further by Su et al. (1996); however, we do not have enough information on this object to present detailed diagnostic diagrams comparable with previous work.

#### 4.2.2 Tentative detections of extended $[\text{P}II]$

A definitive test would be the detection of the  $[\text{P}II]$  line in the extended emission line region. In Figure 9 an extraction is shown of  $0''.7$  of the slit in the region where the  $[\text{FeII}]$  line is strongest, just behind the southeastern radio lobe of Mkn 34.

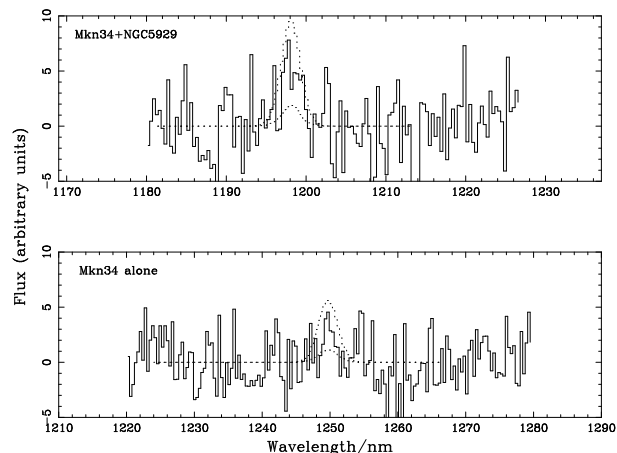


**Figure 9.** (Bottom panel) Area around the  $[\text{P}II]$  line in the six pixels ( $0''.7$ ) near the southeastern radio lobe of Mkn 34 with the strongest  $[\text{FeII}]$  emission. The *predicted*  $[\text{P}II]$  emission, deduced from scaling the  $[\text{FeII}]$  emission by the known wavelength ratio and by scaling in intensity by factors of 4 and 20, is shown by dotted lines. The wavelength scale is that of the observed frame in Mkn 34. (Top panel) Combined extranuclear emission from near to the southeastern radio lobe of Mkn 34, as above, and the region of  $0''.6$  around the southwestern radio lobe of NGC 5929. Both of these regions have enhanced  $[\text{FeII}]$  emission. The spectra have been coadded and corrected to the same wavelength scale by use of the  $[\text{FeII}]$  line. The predicted position of the  $[\text{P}II]$  line is shown in each case; the dotted lines show the  $[\text{P}II]$  line as it would appear if it were factors of 4 and 20 weaker than  $[\text{FeII}]$ . The wavelength scale is that of the observed frame of NGC 5929.

The  $[\text{FeII}]$  line in this region has been fitted with a Gaussian, and is shown shifted to the  $[\text{P}II]$  wavelength and divided in intensity by factors of 4 and 20. There is a spike at exactly the expected wavelength, although it is extremely close to the noise level. If this is real, it clearly indicates that the mechanism operating in this extended region is photoionization, with little or no shock contribution. Unfortunately the signal-to-noise in this spectrum is just too low to make a definite statement.

However, repeating this exercise in the extended region of NGC 5929 associated with the southwestern radio lobe (Figure 5) and in which the  $[\text{FeII}]$  is also enhanced over its value in the nuclear region, reveals a similar *very* marginal  $[\text{P}II]$  detection in the extended emission. Adding the two together, with the appropriate scaling in wavelength (Figure 9) gives a more secure detection of the extended  $[\text{P}II]$  at a level of about 0.2 times the strength of the extended  $[\text{FeII}]$  line. This suggests, somewhat surprisingly, and despite the association with the radio jet, that the dominant mechanism of line excitation in these regions is still photoionization rather than shock excitation.

## 5 CONCLUSIONS

A number of near-IR studies of Seyfert galaxies with extended optical emission have now been carried out, in particular Mkn 78 (Ramos Almeida et al. 2006 and this work), Mkn 34 and NGC 1068 (Oliva et al. 2001). The picture which emerges with reasonable consistency is that the nuclear regions are almost certainly dominated by photoionization by

UV photons, consistent with a mechanism involving the active nucleus. This is indicated both by the ability of photoionization to reproduce observed emission line ratios, and specifically by the inconsistency of the [FeII]/[PII] diagnostic with the enhanced ratios expected from shock models. In the extended emission regions which coincide with radio jets, there is a consistent pattern of changes in emission line ratio consistent with compression of the gas by the bow-shock associated with radio emission. Tentative detections of [PII] in these regions, however, suggest that photoionization is still the dominant mechanism. The fact that the peak line emission is slightly behind the head of the radio jet in Mkn 34 may suggest that the gas has been compressed by the shocks but ionized by the active nucleus after the [FeII] has been returned to the gas phase, rather than by UV and X-ray photons from the shocks themselves. In this case the fact that NGC 5929's peak of [FeII] is coincident with the radio lobe could indicate that the shock compression of the gas has occurred more recently. It is important to confirm these determinations in other objects, using longer integrations on large (8-m class) telescopes.

## ACKNOWLEDGMENTS

Based on observations obtained at the Gemini Observatory, which is operated by the Association of Universities for Research in Astronomy, Inc., under a cooperative agreement with the NSF on behalf of the Gemini partnership: the National Science Foundation (United States), the Particle Physics and Astronomy Research Council (United Kingdom), the National Research Council (Canada), CONICYT (Chile), the Australian Research Council (Australia), CNPq (Brazil) and CONICET (Argentina). RJB acknowledges financial support from the European Commission's I3 Programme "RADIONET" under contract No. 505818. The VLA is operated by the National Radio Astronomy Observatory which is a facility of the National Science Foundation operated under cooperative agreement by Associated Universities, Inc. We thank the observers, I. Song and S. Knights and the operators, B. Walls and G. Tranco, for carrying out the observations.

## REFERENCES

- Alonso-Herrero A., Rieke M.J., Rieke G.H., Ruiz M., 1997, *ApJ*, 482, 747
- Baars, J. W. M., Genzel, R., Pauliny-Toth, I. I. K., Witzel, A., 1977, *A&A*, 61, 99
- Bower G.A., Wilson A.S., Mulchaey J.S., Miley G.K., Heckman T.M., Krolik J.H., 1994, *AJ*, 107, 1686
- Cole G.H.C., Pedlar A., Mundell C.G., Gallimore J.F., Holloway A. J., 1998, *MNRAS*, 301, 782
- Dopita M.A., Sutherland R.S. 1995, *ApJ*, 455, 468.
- Falcke H., Wilson A.S., Simpson C., 1998. *ApJ*, 502, 199.
- Ferland G., Korista K.T., Verner D.A., Ferguson J.W., Kingdon J.B., Verner E.M., 1998. *PASP*, 110, 761
- Forbes D.A., Ward M.J. 1993, *ApJ*, 416, 150.
- Hodapp K.W., Jensen J.B., Irwin E.M., Yamada H. Chung R. Fletcher K. Robertson L. Hora J.L., Simons D.A., Mays W. 2003, *PASP*, 115, 1388.
- Horne K., 1986. *PASP* 98, 609
- Mouri H., Kawara K., Taniguchi Y., 2000, *ApJ*, 528, 186.
- Oliva E., Marconi A., Maiolino R., Testi L., Mannucci F., Ghinassi F., Licandro J., Origlia, L., Baffa, C., Checcucci, A., 2001, *A&A*, 369L, 5.
- Pedlar A., Harrison B., Unger S.W., Graham D.A., Preuss E., Saikia D.J., Yates G.J. 1988, *LNP*, 307, 310.
- Perryman M.A.C., 1997. The Hipparcos and Tycho catalogues. Astrometric and photometric star catalogues derived from the ESA Hipparcos Space Astrometry Mission, Noordwijk, Netherlands, ESA Publications Division, 1997, ESA SP Series vol. 1200.
- Press W.H., Teukolsky S.A., Vetterling W.T., Flannery B.P., 1992. *Numerical Recipes in C*, Cambridge University Press, Cambridge.
- Ramos Almeida C., Pérez-García A.M., Acosta-Pulido J.A., Rodríguez-Espinosa J.M., Barrena R., Manchado A., 2006. *ApJ* 645, 148
- Riffel R., Rodríguez-Ardila A., Pastoriza M.G., 2006, *A&A* 457, 61
- Rodríguez-Ardila A., Pastoriza M.G., Viegas S., Sigut T.A.A., Pradhan A.K., 2004, *A&A*, 425, 457
- Rodríguez-Ardila A., Riffel R., Pastoriza M.G., 2005, *MNRAS*, 364, 1041
- Simpson, C. Forbes, D.A., Baker, A.C., Ward, M.J. 1996, *MNRAS*, 283, 777.
- Su B.M., Muxlow T.W.B., Pedlar A., Holloway A.J., Steffen W., Kukula M.J., Mutel R.L. 1996, *MNRAS*, 279, 1111.
- Sutherland R.S., Bicknell G.V., Dopita M.A. 2003, *ApJ*, 591, 238.
- Ulvestad J.S., Wilson A.S. 1984, *ApJ*, 278, 544.
- Whittle M., Wilson A.S. 2004, *AJ*, 127, 606.
- Whittle M., Pedlar A., Meurs E.J.A., Unger S.W., Axon D.J., Ward M.J. 1988, *ApJ*, 326, 125.
- Whittle M., Silverman J.D., Rosario D.J., Wilson A.S., Nelson C.H., 2004, I.A.U. Symp. 222 "The interplay among black holes, stars and ISM in galactic nuclei", Gramado, Brazil. March 2004, Eds. T. Storchi-Bergmann, L. C. Ho and H. R. Schmitt. p299-302
- Whittle M., Rosario D.J., Silverman J.D., Nelson C.H., Wilson A.S. 2005, *AJ*, 129, 104.